A PLANETARY COMPANION TO HD 40979 AND ADDITIONAL PLANETS ORBITING HD 12661 AND HD 38529[1]

DEBRA A. FISCHER,[2] GEOFFREY W. MARCY,[2] R. PAUL BUTLER,[3] STEVEN S. VOGT,[4] GREGORY W. HENRY,[5]
DIMITRI POURBAIX,[6] BERNARD WALP,[2,4] ANTHONY A. MISCH,[4] AND JASON T. WRIGHT[2]

ABSTRACT

We report the detection of three extrasolar planets from the Lick and Keck observatories. The F8 V star HD 40979 has a companion with orbital period $P = 263.1 \pm 3$ days, eccentricity $e = 0.25 \pm 0.05$, and velocity semiamplitude $K = 101.2 \pm 5.6$ m s^{-1}. The inferred semimajor axis is 0.83 AU and $M \sin i = 3.28 M_{\rm Jup}$. Observations of planetary companions orbiting the G6 V star HD 12661 and the G4 IV star HD 38529 have already been published, and here we report additional, longer period companions for both of these stars. The outer companion to HD 12661 has $P_c = 1444.5 \pm 12.5$ days, $e_c = 0.20 \pm 0.04$, and $K_c = 27.6 \pm 2.5$ m s^{-1}. Adopting a stellar mass of 1.07 $M_\odot$, we find $M_c \sin i = 1.57 M_{\rm Jup}$ and a semimajor axis of 2.56 AU. The second companion to HD 38529 has $P_c = 2174 \pm 30$ days, $e_c = 0.36 \pm 0.05$, and $K_c = 170.5 \pm 9$ m s^{-1}. The assumed mass of 1.39 $M_\odot$ for HD 38529 yields $M_c \sin i = 12.7 M_{\rm Jup}$ and a semimajor axis of 3.68 AU. Photometric observations at Fairborn Observatory reveal low-amplitude brightness variations in HD 40979 and HD 38529 due to rotational modulation in the visibility of photospheric starspots, and they yield rotation periods of 7.0 and 35.7 days, respectively, very different from the planetary orbital periods. The orbital parameters of these two systems are compared with updated parameters for all of the known multiple-planet systems. Updated velocities are provided for the ϒ Andromedae system.

Subject headings: planetary systems — stars: individual (HD 12661, HD 38529, HD 40979) — stars: low-mass, brown dwarfs

On-line material: machine-readable tables

1. INTRODUCTION

About 100 extrasolar planets[7] have been discovered orbiting solar-type stars (see references in Butler et al. 2003) using high-precision Doppler observations to measure the reflex radial velocity of the host star induced by unseen planetary companions. The first planets detected by Doppler observations resided in relatively short period orbits (e.g., 51 Peg; Mayor & Queloz 1995). Now, with a time baseline of several years, virtually all of the short-period gas giant planets in current Doppler stellar samples have been detected, and planets with orbital periods of 1 or more years are emerging.

The first multiple-planet system orbiting a main-sequence star other than the Sun was discovered in 1999 (Butler et al. 1999) orbiting ϒ Andromedae. One interesting characteristic of extrasolar planets that has emerged in the past 2 years is that these multiple-planet systems appear to be common. In addition to the triple-planet system orbiting ϒ And, double-planet systems have been published for HD 168443 (Marcy et al. 2001b), GJ 876 (Marcy et al. 2001a), 47 UMa (Fischer et al. 2002), and HD 37124 (Butler et al. 2003). Recently, another triple-planet system was discovered orbiting 55 Cnc (Marcy et al. 2002). Fischer et al. (2001) showed that five of 12 planet-bearing stars on the Lick survey exhibited residual velocities to a single planet fit that indicated the presence of additional planets. The number of probable multiple-planet systems among those dozen Lick stars has since increased from five to seven. The multiple-planet systems offer a unique opportunity to investigate dynamical interactions and planet resonances (Marcy et al. 2001a; Lee & Peale 2002; Laughlin & Chambers 2001; Rivera & Lissauer 2001; Marcy et al. 2002) and to understand the conditions in the evolving protoplanetary disk (Chiang & Murray 2002; Ford et al. 2003).

2. OBSERVATIONS

We are carrying out a Doppler survey of about 350 stars at Lick Observatory and 600 stars at Keck Observatory. Stars with velocity variations at Lick Observatory are generally added to the Keck survey to increase both phase coverage and velocity precision. Velocity precision at Lick Observatory is generally photon-limited. The consistently higher signal-to-noise ratio (S/N) observations at Keck result in velocity precision that is almost uniformly a few meters per second for chromospherically inactive stars.

The Hamilton spectrograph (Vogt 1987) at Lick Observatory has a resolution $R \approx 50,000$ and is fed with light from

[2] Department of Astronomy, University of California at Berkeley, 601 Campbell Hall, Berkeley, CA 94720; fischer@serpens.berkeley.edu.

[3] Department of Terrestrial Magnetism, Carnegie Institution of Washington, 5241 Broad Branch Road NW, Washington, DC 20015-1305.

[4] University of California Observatory/Lick Observatory, University of California at Santa Cruz, Santa Cruz, CA 95064.

[5] Center of Excellence in Information Systems, Tennessee State University, 330 10th Avenue North, Nashville, TN 37203; Senior Research Associate, Department of Physics and Astronomy, Vanderbilt University, Nashville, TN 37235.

[6] Research Associate, FNRS, Belgium, Institut d'Astronomie et d'Astrophysique, Université Libre de Bruxelles CP 226, Boulevard du Triomphe, B-1050 Brussels, Belgium.

[7] Updates on orbital parameters can be found at http://exoplanets.org.

either the Shane 3 m Telescope or the 0.6 m coudé auxiliary telescope (CAT). The typical S/N for $V = 7$ stars is 140 pixel^{-1} for either a single 10 minute observation with the 3 m telescope or for two 40 minute observations with the CAT. The HIRES spectrograph (Vogt et al. 1994) at Keck has a resolution $R \approx 70,000$. Exposure times for stars brighter than $V = 7$ are typically 2 minutes and yield S/Ns better than 200.

The Hamilton spectral format spans a wavelength range of 3700–9000 Å, and the Keck spectral format spans a wavelength range of 3700–6200 Å. Both projects employ an iodine cell to impose a grid of sharp reference lines between 5000 and 6000 Å on the stellar spectrum. In the analysis, a high-S/N template spectrum without iodine is combined with a Fourier transform spectrometer iodine observation to model instrumental broadening and to derive differential radial velocities in the observations of the star with iodine (Butler et al. 1996). The velocities for all three stars in this paper made use of a high-resolution, high-S/N template spectrum from Keck.

Strong magnetic fields can produce stellar spots in young active stars that introduce shifting line asymmetries (Saar, Butler, & Marcy 1998). In the most extreme cases, shifting line centroids can masquerade as dynamical Doppler variations (Queloz et al. 2001). However, for inactive stars, the chromospheric contribution to velocity noise is empirically less than 3 m s^{-1}. We measure core emission in the Ca II H and K lines to assess the chromospheric activity level of all planet search targets. The H and K core emission is characterized by a pseudo–equivalent width, or S_{HK}, index, analogous to the Mount Wilson HK project (Baliunas et al. 1998). The S index is then transformed to log R'_{HK}, a ratio of the HK flux to the bolometric flux of the star. This index is a good predictor of the rotational period (Noyes et al. 1984) and the approximate age of F, G, and K main-sequence stars (Baliunas et al. 1995).

Photometric observations were obtained of HD 40979 and HD 38529 with the T11 and T12 0.8 m automatic photoelectric telescopes (APTs) at Fairborn Observatory.[8] These APTs measure the difference in brightness between a program star and nearby comparison stars in the Strömgren b and y passbands. The observing procedures and data reduction techniques employed with the T11 and T12 APTs are identical to those for the T8 0.8 m APT described in Henry (1999). The external precision of the photometric observations, defined as the standard deviation of a single differential magnitude from the seasonal mean of the differential magnitudes, is typically around 0.0012 mag for these telescopes, as determined from observations of pairs of constant stars.

2.1. HD 40979

HD 40979 (=HIP 28767) is a $V = 6.74$, $B-V = 0.573$, F8 V star. The *Hipparcos* parallax (Perryman 1997) of 30 mas implies a distance of 33 pc and absolute visual magnitude $M_V = 4.12$. Allende Prieto & Lambert (1999) use the *Hipparcos* parallax, together with evolutionary tracks, to derive a stellar mass of 1.0 $M_\odot$ and a stellar radius of 1.26 $R_\odot$. This combination of stellar mass and radius suggests that the star is a slightly evolved G0 IV star. However, that assessment is

not consistent with the $B-V$ color of the star, the Ca II H and K emission, or the strong lithium feature. We measure a lithium abundance $N(Li) = 2.79$ for HD 40979. If the star were really 1 $M_\odot$, this lithium abundance would indicate that the star is about the age of the Hyades (see, e.g., Jones, Fischer, & Soderblom 1999), but in that case, the Ca H and K emission should be stronger. If instead, the star is 1.1–1.2 $M_\odot$ with an age of about 1.5 Gyr, then the lithium abundance, the $B-V$ color, and the measured Ca H and K emission are all consistent with expected values.

Spectral synthesis modeling yields $T_{eff} = 6095 \pm 30$ K, $[Fe/H] = 0.194 \pm 0.05$, and $v \sin i = 7.4 \pm 0.5$ km s^{-1}. Accounting for the increased metallicity, we estimate a stellar mass of 1.1 $M_\odot$. Our measurement of $S_{HK} = 0.237$ (on the Mount Wilson scale) yields log $R'_{HK} = -4.63$, indicating moderate chromospheric activity in HD 40979 and an estimated rotational period of 8.9 days. The Ca II H line for HD 40979 is compared to the solar spectrum in the top panel of Figure 1. The stellar characteristics of HD 40979 and the other two stars in this paper are summarized in Table 1.

HD 40979 has been observed at Lick Observatory since 1998 with an average S/N of 135 and velocity precision of about 12 m s^{-1}. At Keck, the typical S/N is 290, and the corresponding velocity precision is about 4.3 m s^{-1}. The Lick data span approximately six orbital periods; however, the initial phase sampling of this star was unlucky in that the stellar velocities were measured near successive minima. Given the moderate $v \sin i$ and chromospheric activity (both increase velocity errors) and the low initial rms velocity scatter, this star was designated as a lower priority target, and the identification of significant velocity variations was delayed until 2000 November. In 2001, HD 40979 was added to the Keck survey.

Forty-five velocities from Lick and Keck (Table 2) have been combined with an offset chosen to minimize residuals to the Keplerian fit. The best Keplerian fit to the combined data (Figs. 2a and 2b) yields an orbital period $P = 263.1 \pm 3$ days, eccentricity $e = 0.25 \pm 0.05$, and velocity semiamplitude $K = 101.2 \pm 5.6$ m s^{-1}. The assumed stellar mass of 1.1 $M_\odot$ implies a companion mass of $M \sin i = 3.28$ M_{Jup} and a semimajor axis of 0.83 AU. The orbital elements for HD 40979 are listed in Table 3.

TABLE 1
STELLAR CHARACTERISTICS

Property	HD 40979	HD 12661	HD 38529
V	6.74	7.43	5.95
$B-V$	0.573	0.71	0.773
Spectral type	F8 V	G6 V	G4 IV
M_V	4.12	4.58	2.81
Distance (pc)	33.3	37.2	42.4
[Fe/H]	0.194	0.293	0.313
T_{eff} (K)	6095	5644	5600
$v \sin i$ (km s^{-1})	7.4	3.08	4.9
M_{star} ($M_\odot$)	1.1	1.07	1.39
R_{star} ($R_\odot$)	1.26	1.09	2.82
S_{HK}	0.237	0.15	0.1926
log R'_{HK}	−4.63	−5.06	−4.89
P_{rot} (days)	7.0[a]	34.2[b]	35.7[a]

[a] Rotation period from direct photometric observations.
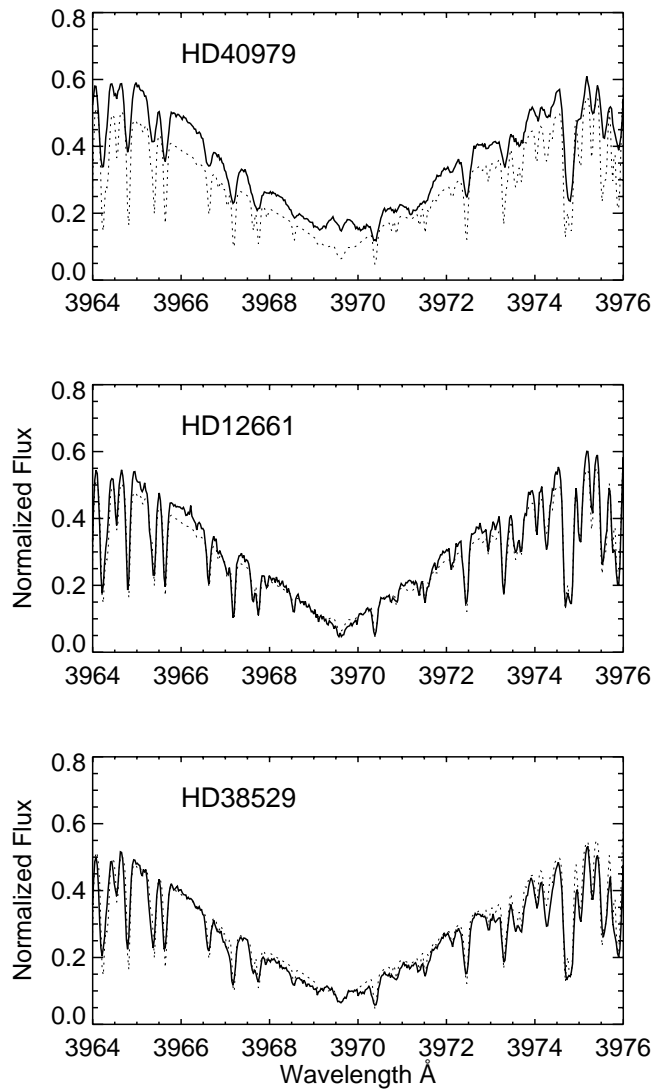[b] Rotation period estimated from Ca H and K emission.

FIG. 1.—Spectra of HD 40979, HD 12661, and HD 38529 near the Ca II H line (*solid line*) with the solar NSO spectrum overplotted (*dotted line*). HD 40979 shows moderate emission; however, the lack of core emission in HD 12661 and HD 38529 indicates that these stars have low chromospheric activity.

TABLE 2
RADIAL VELOCITIES FOR HD 40979

JD − 2,440,000	RV (m s^{-1})	Uncertainties (m s^{-1})	Observatory
10,831.772..........	2.29	18.69	Lick
11,175.953..........	−39.27	18.33	Lick
11,859.977..........	138.15	11.92	Lick
11,860.944..........	83.16	12.15	Lick
11,998.688..........	−54.17	11.30	Lick
12,000.667..........	−35.11	10.54	Lick
12,001.678..........	0.67	12.09	Lick
12,028.674..........	−26.87	19.59	Lick
12,033.670..........	9.64	7.28	Lick
12,040.677..........	33.18	9.76	Lick
12,041.676..........	26.05	13.18	Lick
12,158.028..........	53.15	12.37	Lick
12,160.030..........	28.08	9.56	Lick
12,161.029..........	46.22	9.15	Lick
12,162.025..........	33.53	9.01	Lick
12,202.027..........	16.37	9.53	Lick
12,203.021..........	−21.45	12.56	Lick
12,203.992..........	0.00	10.50	Lick
12,205.040..........	−35.51	12.93	Lick
12,217.970..........	−33.33	11.11	Lick
12,218.924..........	−26.98	12.33	Keck
12,220.106..........	−27.91	5.62	Lick
12,221.005..........	−31.51	12.77	Keck
12,221.969..........	−42.97	9.43	Lick
12,235.967..........	−45.70	4.05	Lick
12,237.903..........	−40.33	3.77	Keck
12,238.908..........	−51.86	4.41	Keck
12,243.003..........	−42.56	4.51	Keck
12,267.845..........	−64.67	7.92	Keck
12,281.938..........	6.87	14.82	Keck
12,282.943..........	−36.18	17.59	Lick
12,285.930..........	−7.89	15.52	Lick
12,287.881..........	−36.61	12.13	Lick
12,299.707..........	20.18	12.13	Lick
12,307.859..........	54.55	4.51	Keck
12,316.758..........	77.68	10.51	Keck
12,333.695..........	171.77	9.19	Lick
12,334.666..........	134.46	10.76	Lick
12,334.815..........	139.86	5.34	Lick
12,335.674..........	127.32	10.66	Keck
12,345.704..........	182.45	13.82	Keck
12,348.655..........	140.65	11.73	Lick
12,534.998..........	−9.31	8.06	Lick
12,536.131..........	−28.74	4.79	Keck
12,537.091..........	−29.72	4.87	Keck

NOTE.—Table 2 is also available in machine-readable form in the electronic edition of the *Astrophysical Journal*.

The reduced $(\chi^2)^{1/2}$ fit for this orbital solution is 1.73, and the rms to the fit is 18.7 m s^{-1}. The rms to the Keplerian fit exceeds the mean velocity errors; however, there is no visible trend in the residual velocities, and a periodogram analysis does not show evidence of additional periodic velocity variations. HD 40979 is illustrative of the drop-off in Doppler information for earlier spectral types: the lines of F-type stars are shallower and broader than for G dwarfs, resulting in relatively high internal velocity errors. The most likely source of the high rms velocity scatter is the moderate level of chromospheric activity (Saar et al. 1998).

HD 40979 was observed during 2002 with the T12 0.8 m APT at Fairborn Observatory as an additional check on its level of surface activity. The differential magnitudes in the combined Strömgren $(b + y)/2$ passband are shown in Figure 3 and are relative to the comparison star HD 41074. The top panel shows our entire data set to date. The most recent observations, between the two dashed vertical lines, are replotted in the middle panel and show the most coherent variability, which we interpret as rotational modulation in the visibility of photospheric starspots. Period analysis of this subset gives a rotation period of 7.0 ± 0.5 days for HD 40979, similar to the rotation period of 8.9 days estimated from the Ca H and K emission but very different from the 263.1 day orbital period of the planetary companion.

The rotation period, stellar radius, and $v \sin i$ can be used to estimate the inclination of the stellar rotation axis. Adopting the stellar radius from Allende Prieto & Lambert (1999) of 1.26 $R_\odot$ suggests that the star is being viewed close to equator-on. In order for the rotation axis to be less than 20° from our line of site (close to pole-on) the stellar radius
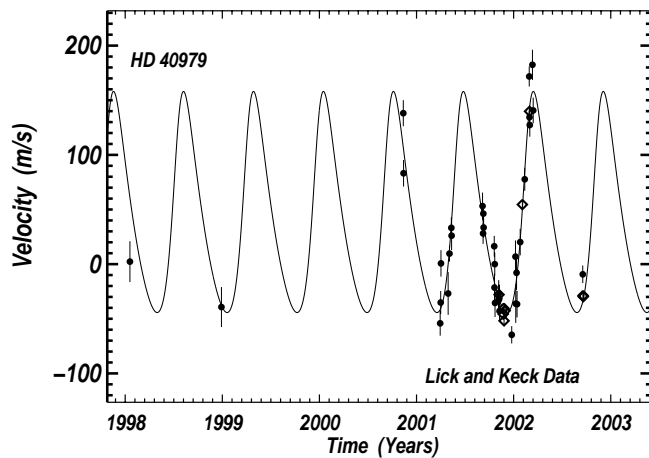
FIG. 2a

FIG. 2b

FIG. 2.—Combined Lick and Keck radial velocities as a function of (a) time and (b) phase for HD 40979. Lick observations are shown as filled circles, and the Keck data are plotted as diamonds. The solid line shows the radial velocity curve from the best-fit orbital solution, $P = 263$ days, $e = 0.25$, and $M \sin i = 3.28\ M_{\mathrm{Jup}}$. The rms to this fit is 18.7 m s^{-1} with a reduced $(\chi^2)^{1/2} = 1.73$.
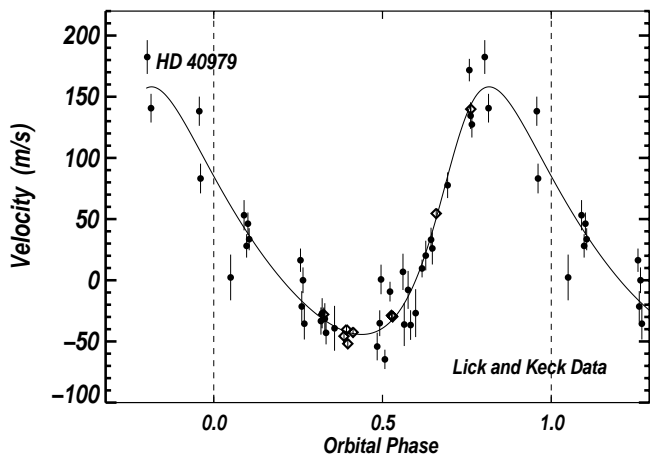
would need to be several times the solar radius or the rotation period would have to be shorter than 3 days. Such extreme values for the stellar radius and rotation period seem physically unreasonable given the observed characteristics of HD 40979. Assuming that the orbital inclination vector is parallel to the rotation axis of the star, the orbital inclination may also be close to 90° (or nearly edge-on).

The *Hipparcos* astrometric solution can rule out the most extreme (low) inclination case, adding an additional constraint on the companion mass to the substellar regime. We adopted the orbital elements for the planetary companion described in this paper and refitted the *Hipparcos* intermediate data for HD 40979. However, this did not improve the original statistical fit. The lack of a detection by *Hipparcos* constrains the astrometric displacement of the star to less than the 2 σ error, or more than 2 mas. Therefore, the mass ratio of the companion to the star must be less than 2 mas divided by the angular separation, or less than 2/27 mas. This sets an upper limit to the companion mass of 0.074 $M_{\odot}$, near the hydrogen-burning (stellar) threshold.

2.2. *HD 12661*

HD 12661 (=HIP 9683) is a $V = 7.43$, $B-V = 0.71$, G6 V star. The *Hipparcos* parallax (Perryman 1997) of 0.0269 mas implies a distance of 37.16 pc and an absolute visual

magnitude of 4.58. Spectral synthesis modeling yields $T_{\mathrm{eff}} = 5644 \pm 30$ K, $[\mathrm{Fe/H}] = 0.293 \pm 0.05$, and $v \sin i = 3.08 \pm 0.5$ km s^{-1}. The Ca II H line, shown in the middle panel of Figure 1, does not exhibit any emission. Our measured $S_{\mathrm{HK}} = 0.15$ corresponds to a chromospherically

TABLE 3
Orbital Parameters for HD 40979

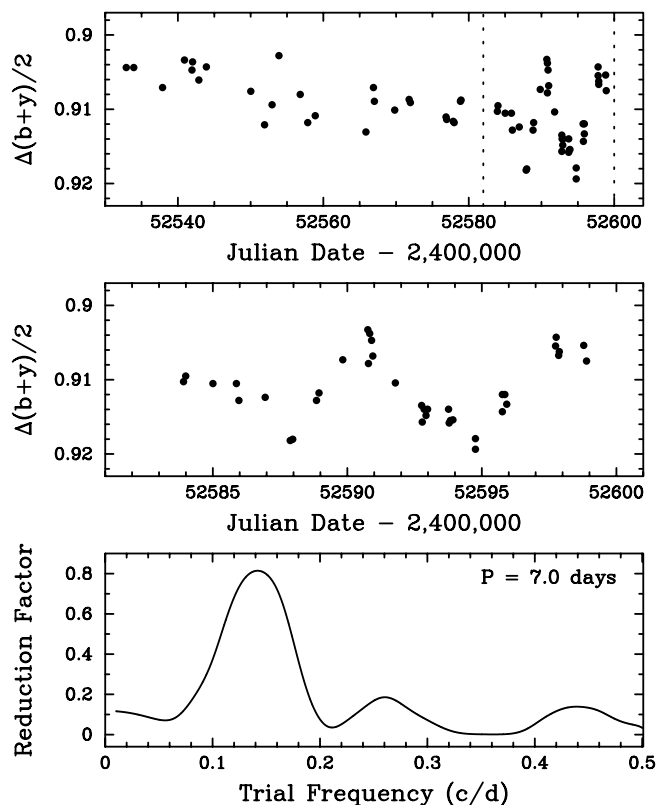| Parameter	HD 40979
P (days)..................	263.1 (3.0)
T_p (JD)....................	2,452,327.2 (17.0)
e..............................	0.25 (0.05)
ω (deg)....................	310.7 (8.0)
K_1 (m s^{-1})................	101.2 (5.6)
$a_1 \sin i$ (AU)...........	2.37E$-$03
$f_1(m)$ ($M_{\odot}$)..............	2.56E$-$08
a_{rel} (AU).................	0.83
$M \sin i$ (M_{Jup})	3.28
N_{obs}.......................	45
rms (m s^{-1}).............	18.7
Reduced $(\chi^2)^{1/2}$.......	1.73

FIG. 3.—Photometry of HD 40979 acquired with the T12 0.8 m APT at Fairborn Observatory. The top panel shows the entire data set. The subset between the dashed vertical lines, replotted in the middle panel, shows the most coherent rotational modulation in the star's brightness. Period analysis of this subset is shown in the bottom panel and reveals a clear rotation signal of 7.0 ± 0.5 days, similar to the 8.9 day rotation period predicted from the star's Ca H and K emission but very different from the planetary orbital period of 263.1 days.

inactive $\log R'_{\rm HK} = -5.06$ and a rotational period of 34.2 days. These stellar characteristics are summarized in Table 1.

An inner planet orbiting HD 12661 was reported by Fischer et al. (2001). At that time, a weak linear trend in the velocity residuals to the single-planet fit was noted. Observations at Lick and Keck (Table 4) now confirm the presence of an outer planet orbiting HD 12661. The revised orbital solution for the inner planet is $P_b = 263.6 \pm 1.2$ days, $e_b = 0.35 \pm 0.03$, and $K_b = 74.4 \pm 1.5$ m s^{-1}. Retaining the estimated stellar mass (Fischer et al. 2001) of 1.07

TABLE 4
RADIAL VELOCITIES FOR HD 12661

JD − 2,440,000	RV (m s^{-1})	Uncertainties (m s^{-1})	Observatory
10,831.608..........	−4.43	11.95	Lick
11,027.001..........	55.99	10.03	Lick
11,154.673..........	−46.18	8.87	Lick
11,155.746..........	−74.79	8.64	Lick
11,170.828..........	−90.11	3.40	Keck
11,171.728..........	−92.88	2.94	Keck
11,172.831..........	−92.16	3.38	Keck
11,173.857..........	−94.34	3.23	Keck
11,206.666..........	−92.94	7.65	Lick
11,226.751..........	−96.85	2.98	Keck
11,227.745..........	−95.41	3.02	Keck
11,228.723..........	−95.56	2.97	Keck
11,445.017..........	−59.84	7.65	Lick
11,445.996..........	−69.61	6.38	Lick
11,446.998..........	−77.97	7.70	Lick
11,498.790..........	−46.71	8.32	Lick
11,501.744..........	−45.14	9.89	Lick
11,533.772..........	60.62	6.21	Lick
11,534.752..........	73.27	8.10	Lick
11,535.714..........	67.30	6.19	Lick
11,536.693..........	61.15	7.17	Lick
11,539.733..........	64.22	6.86	Lick
11,540.699..........	69.58	6.40	Lick
11,550.757..........	71.88	3.14	Keck
11,551.784..........	71.30	2.79	Keck
11,552.787..........	73.88	4.10	Keck
11,580.732..........	49.19	3.11	Keck
11,581.791..........	46.58	3.08	Keck
11,581.637..........	54.16	17.48	Lick
11,585.715..........	40.03	3.17	Keck
11,750.979..........	−49.45	5.73	Lick
11,752.983..........	−37.91	4.66	Lick
11,757.053..........	−39.53	3.29	Keck
11,774.973..........	0.21	4.17	Lick
11,776.002..........	−1.86	4.13	Lick
11,805.971..........	100.58	10.11	Lick
11,860.790..........	56.84	6.64	Lick
11,883.920..........	27.89	3.42	Keck
11,898.973..........	6.64	2.77	Keck
11,899.880..........	8.57	2.92	Keck
11,900.858..........	6.64	3.13	Keck
11,913.698..........	1.83	5.93	Lick
11,914.658..........	1.81	3.73	Lick
11,915.663..........	0.00	3.81	Lick
11,927.646..........	−14.18	5.23	Lick
11,945.655..........	−27.34	4.96	Lick
11,946.666..........	−22.09	4.03	Lick
11,973.712..........	−41.74	2.74	Keck
12,098.105..........	82.47	3.92	Keck
12,099.121..........	74.77	3.57	Keck

TABLE 4—Continued

JD − 2,440,000	RV (m s^{-1})	Uncertainties (m s^{-1})	Observatory
12,100.115..........	85.42	4.22	Keck
12,121.960..........	61.33	6.40	Lick
12,122.995..........	47.48	7.55	Lick
12,129.088..........	43.39	3.31	Keck
12,133.122..........	49.23	3.68	Keck
12,134.006..........	35.56	3.56	Keck
12,157.958..........	31.15	6.57	Lick
12,160.969..........	23.46	7.05	Lick
12,161.944..........	16.35	6.48	Lick
12,162.924..........	12.21	3.50	Keck
12,189.125..........	−8.05	3.83	Keck
12,219.036..........	−37.10	3.53	Keck
12,235.726..........	−55.21	3.40	Keck
12,236.822..........	−55.25	3.14	Keck
12,238.773..........	−55.17	2.95	Keck
12,241.675..........	−66.01	5.75	Keck
12,242.846..........	−61.49	3.06	Keck
12,287.744..........	−54.16	14.29	Lick
12,299.649..........	−27.68	3.75	Keck
12,302.720..........	−7.58	8.04	Lick
12,307.748..........	20.09	2.42	Keck
12,314.635..........	7.77	12.50	Lick
12,315.641..........	30.57	8.68	Lick
12,316.629..........	52.42	10.79	Lick
12,333.673..........	74.23	6.88	Lick
12,334.792..........	85.24	2.61	Keck
12,334.637..........	74.47	7.72	Lick
12,493.991..........	−88.25	3.60	Keck
12,508.996..........	−95.33	4.09	Keck
12,512.010..........	−88.46	5.39	Keck
12,512.991..........	−84.66	4.06	Keck
12,513.973..........	−90.72	4.07	Keck
12,515.136..........	−89.88	3.20	Keck
12,515.946..........	−88.80	3.38	Keck
12,535.940..........	−85.60	3.31	Keck
12,536.949..........	−85.90	3.62	Keck

NOTE.—Table 4 is also available in machine-readable form in the electronic edition of the *Astrophysical Journal*.

$M_\odot$, we derive a semimajor axis $a_b = 0.83$ AU and $M_b \sin i = 2.30 M_{\rm Jup}$. The orbital parameters for the outer planet are $P_c = 1444.5 \pm 12.5$ days, $e_c = 0.20 \pm 0.04$, $K_c = 27.6 \pm 2.5$ m s^{-1}, $a_c = 2.56$ AU, and $M_c \sin i = 1.57 M_{\rm Jup}$. The updated orbital parameters for both planets are listed in Table 5.

TABLE 5
ORBITAL PARAMETERS FOR HD 12661

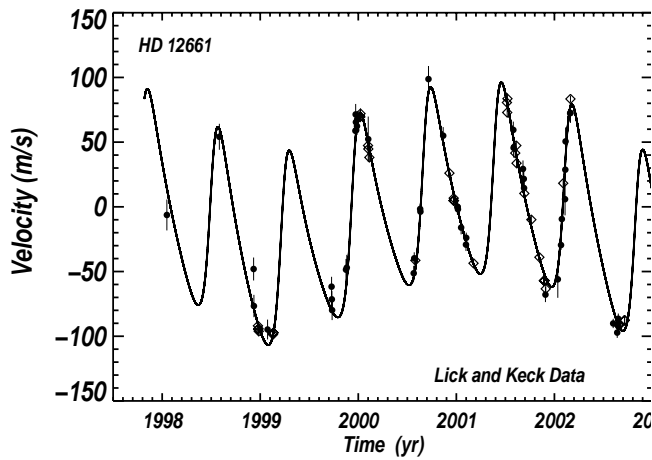| Parameter	HD 12661b	HD 12661c
P (days)...................	263.6 (1.2)	1444.5 (12.5)
T_p (JD)....................	2,449,941.9 (6.2)	2,449,733.6 (49.0)
e............................	0.35 (0.03)	0.20 (0.04)
ω (deg).....................	293.1 (5.0)	162.4 (18.5)
K_1 (m s^{-1})...............	74.4 (1.5)	27.6 (2.5)
$a_1 \sin i$ (AU)...........	1.69E−03	3.59E−03
$f_1(m)$ ($M_\odot$)..............	9.24E−09	2.96E−09
$a_{\rm rel}$ (AU).................	0.83	2.56
$M \sin i$ ($M_{\rm Jup}$)	2.30	1.57
$N_{\rm obs}$.......................	...	86
rms (m s^{-1}).............	...	8.8
Reduced $(\chi^2)^{1/2}$.......	...	1.46

Fig. 4.—Combined Lick and Keck radial velocities for HD 12661. The Lick observations are again shown as filled circles and, the Keck observations are plotted as diamonds. The solid line shows the best double-Keplerian fit to the data, $P_b = 264$ days, $e_b = 0.35$, $M_b \sin i = 2.3\ M_{\rm Jup}$ and $P_c = 1445$ days, $e_c = 0.2$, $M_c \sin i = 1.57\ M_{\rm Jup}$. The rms to this fit is 8.8 m s^{-1} with a reduced $(\chi^2)^{1/2} = 1.46$.

The double-planet Keplerian solution was determined with two different fitting algorithms. First, an initial estimate of the orbital elements was obtained by fitting and subtracting the dominant Keplerian variation (here, the 263 day period) and then fitting the residuals with a second Keplerian. Several iterations of this two-step scheme were carried out to refine the match between a simple superposition of two Keplerian solutions and the observations. Then, these orbital elements were used as initial guesses in a second algorithm that utilized Levenberg-Marquardt minimization between the observations and a double-Keplerian model with 11 free orbital parameters. The orbital elements derived with each of the two fitting routines agree within the stated Monte Carlo uncertainties (discussed below). Table 5 lists the orbital elements obtained with the latter fitting routine, and Figure 4 shows the fit of this double-Keplerian model to the data. In Figures 5a and 5b, the individual components of the double-Keplerian system are revealed by subtracting theoretical velocities for the outer and inner companions, respectively.

The formal errors in the orbital parameters were estimated with Monte Carlo simulations in which Gaussian noise was scaled to the actual errors and then added to the original velocities. The Monte Carlo velocities were then run through the double-Keplerian fitting code, and the standard deviations of the orbital elements in these trials were adopted as our formal errors. The true uncertainty in the orbital period of the outer companion to HD 12661 (P_c) is tied to the fact that the early phase coverage was sparse, and only a single orbit has been observed. Therefore, the Monte Carlo errors are likely to underestimate our true uncertainty in P_c. A more precise orbit for the outer planet will require at least one additional season of data.

The semimajor axis of the outer companion, 2.5 AU, or 0″067, would have given rise to the most detectable astrometric signature in this double-planet system. We refitted the *Hipparcos* data to include the outer Doppler companion; however, this did not result in an improved χ^2 fit to the astrometric data. The stated error in the *Hipparcos* parallax and proper-motion solution for HD 12661 is 0.8 mas for 52 measurements spanning the 4 yr mission lifetime. Adopting a $2\,\sigma$ astrometric error of 1.6 mas, this null observation places an upper limit on the mass ratio $M_{\rm pl}/M_{\rm star} < 1.6/67$, placing a mild constraint on the companion mass: $1.57 M_{\rm Jup} < M_{\rm pl} < 25 M_{\rm Jup}$. Since the *Hipparcos* mission lifetime was comparable to the orbital period of the outer companion, a companion more massive than about $25 M_{\rm Jup}$ would have exhibited a detectable signal.

2.3. *HD 38529*

HD 38529 (=HIP 27253) is a $V = 5.95$, $B-V = 0.773$, G4 IV star. The *Hipparcos* parallax (Perryman 1997) is 23.57 mas, corresponding to a distance of 42.4 pc and absolute visual magnitude $M_v = 2.81$. Using spectral synthesis modeling, we find $T_{\rm eff} = 5600 \pm 30$ K, [Fe/H] $= 0.36 \pm 0.05$, and $v \sin i = 4.4 \pm 0.5$ km s^{-1}. The Ca II H line is plotted in the bottom panel of Figure 1 and demonstrates the low chromospheric activity level of the star. The measured $S_{\rm HK} = 0.193$ is used to derive $\log R'_{\rm HK} = -4.89$ and a rotational period of 34.5 days. We retain the stellar mass of 1.39 $M_\odot$ from Fischer et al. (2001). HD 38529 is the most massive planet-bearing star known to date. The main-sequence progenitor of this star was probably of spectral type about F5.
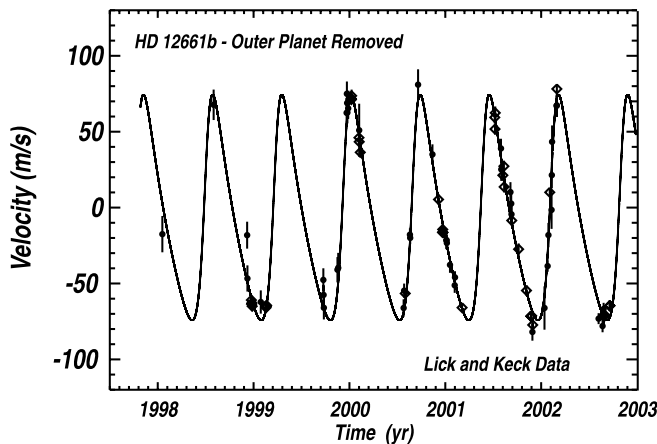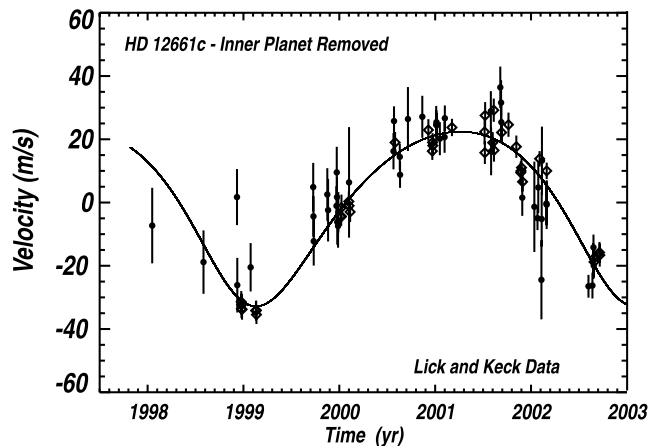

Fig. 5a

Fig. 5b

Fig. 5.—Lick and Keck radial velocities of HD 12661 after (a) subtracting the Keplerian fit to the outer planet and (b) subtracting theoretical velocities for the inner planet. The solid lines show the single-Keplerian model for each component.
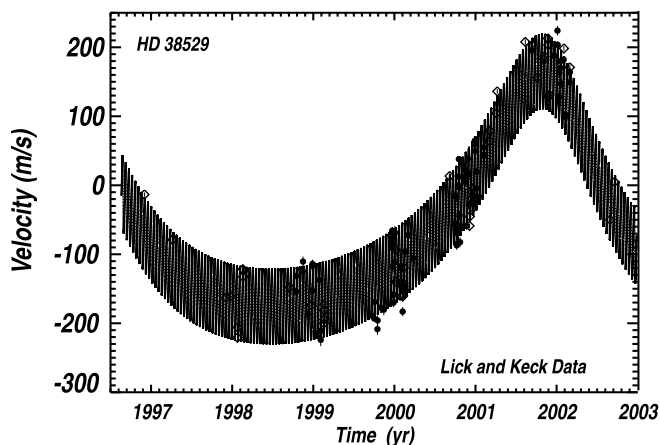
FIG. 6.—Combined Lick and Keck radial velocities for HD 38529. The solid line shows the best-fit double-Keplerian model, $P_b = 14.3$ days, $e_b = 0.29$, $M_b \sin i = 0.78 M_{\rm Jup}$ and $P_c = 2174$ days, $e_c = 0.36$, $M_c \sin i = 12.7 M_{\rm Jup}$. The rms to this fit is 11 m s^{-1} with a reduced $(\chi^2)^{1/2} = 2.08$.

As a main-sequence star, it would have been difficult to achieve the velocity precision that we now observe for HD 38529 as a subgiant. The intrinsic stellar characteristics of this star are included in Table 1.

A planet with an orbital period of 14.3 days was reported in Fischer et al. (2001). A long-period residual trend was noted in that paper and attributed to a more distant companion. The outer companion has completed one full orbit, and the velocities (listed in Table 6) are well described by a double-Keplerian orbital model. The double-Keplerian orbital solution and uncertainties (listed in Table 7) were determined in the same manner described above for HD 12661. The inner companion has an orbital period $P_b = 14.309 \pm 0.050$ days, $e_b = 0.29 \pm 0.02$, and $K_b = 54.2 \pm 1.2$ m s^{-1}. The stellar mass of 1.39 $M_\odot$ yields $a_b = 0.129$ AU and $M_b \sin i = 0.78 M_{\rm Jup}$. The outer companion has $P_c = 2174 \pm 30$ days, $e_c = 0.36 \pm 0.05$, $K_c = 170.5 \pm 9$ m s^{-1}, $a_c = 3.68$ AU, and $M \sin i = 12.7 M_{\rm Jup}$. This strongly suggests that the outer companion is massive

enough to burn deuterium and thus may be more accurately categorized as a brown dwarf. The double-Keplerian fit is shown in Figure 6. Theoretical velocities were calculated for the individual components and subtracted to show the fits to each planet separately in Figures 7a and 7b.

The discovery paper for the inner planet, HD 38529, noted an acceleration solution in *Hipparcos* indicative of a companion with a period of roughly 10 yr. The Double and Multiple Systems Annex notes accelerations in proper motions of -4.17 ± 3.00 mas yr^{-2} (in right ascension) and 7.31 ± 2.09 mas yr^{-2} (in declination). We refitted the *Hipparcos* intermediate astrometric data and initially found significant improvement in the χ^2 fit when the orbital model was included. However, this initial improvement was subsequently found to be spurious: strong correlations in the *Hipparcos* solution were discovered that increased uncertainties in the proper motion so that the statistical fit improved. To eliminate these correlations, the more accurate proper-motion solution from Tycho 2 (Høg et al. 2000) was adopted. This reanalysis still shows an astrometric acceleration term; however, this does not appear to arise from the outer companion presented here.

We have also monitored HD 38529 for brightness variations over the last two observing seasons with the T11 0.8 m APT (Fig. 8). The photometric observations in the combined Strömgren $(b + y)/2$ bandpass are relative to the comparison star HD 37788. The star appeared photometrically quiet without periodicity in the power spectrum of the first season of data. However, the mean magnitude shifted by a few millimagnitudes in the second season, suggesting multiyear variability. Furthermore, a subset of photometry taken during the second season showed variability with a periodicity of 35.7 days, consistent with the rotation period of the star (middle panel, Fig. 8). It seems unlikely that the observed photometric variability can explain the 14.3 day Doppler variations. First, the velocity phase coverage is excellent, so we are not fitting an alias of the longer period photometric periodicity. Second, the 14.3 day velocity signal persists in the entire 5 yr data set, while the photometric coherence is only present over two consecutive 35 day cycles during two seasons of data. And third, the relatively large amplitude of the velocity variation, 55 m s^{-1}, is unlikely to
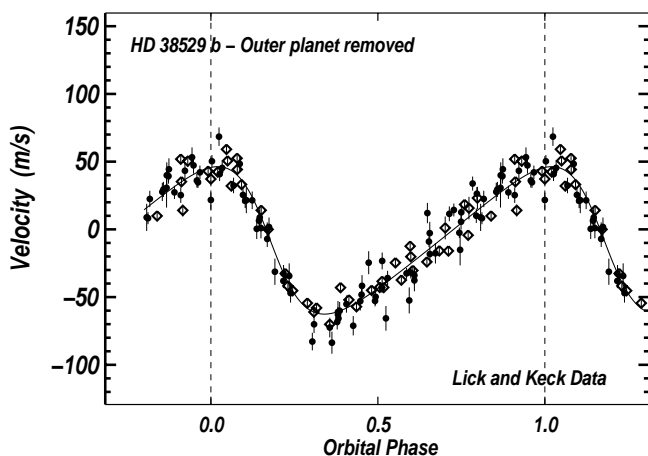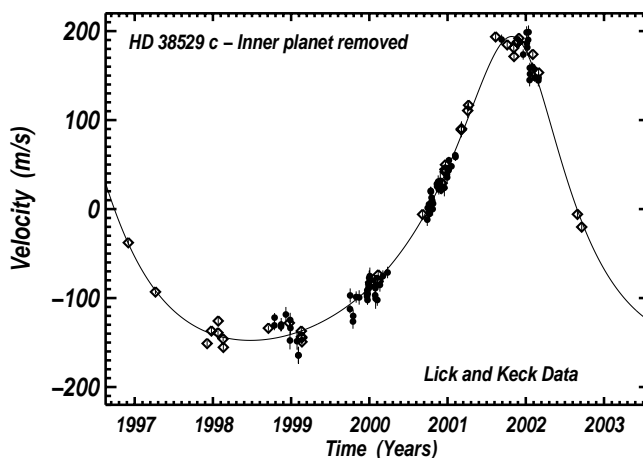

FIG. 7a

FIG. 7b

FIG. 7.—Lick and Keck radial velocities of HD 38529 after (a) subtracting the Keplerian fit to the outer planet and (b) subtracting theoretical velocities for the inner planet. The solid lines show the single-Keplerian model for each component.

TABLE 6
RADIAL VELOCITIES FOR HD 38529

JD − 2,440,000	RV (m s^{-1})	Uncertainties (m s^{-1})	Observatory
10,418.959..........	45.46	2.98	Keck
10,545.771..........	−20.04	2.90	Keck
10,787.014..........	−104.36	2.98	Keck
10,807.062..........	−101.83	3.33	Keck
10,837.758..........	−162.10	2.78	Keck
10,838.784..........	−147.19	3.52	Keck
10,861.730..........	−62.61	2.95	Keck
10,862.725..........	−73.59	2.85	Keck
11,073.059..........	−89.17	3.00	Keck
11,101.025..........	−95.03	5.44	Lick
11,102.022..........	−72.61	5.17	Lick
11,131.920..........	−65.70	5.56	Lick
11,132.929..........	−51.75	7.29	Lick
11,154.808..........	−128.30	8.48	Lick
11,170.895..........	−115.10	2.93	Keck
11,173.915..........	−93.62	10.04	Lick
11,174.868..........	−58.03	8.09	Lick
11,175.922..........	−55.09	6.12	Lick
11,206.805..........	−78.49	9.56	Lick
11,212.786..........	−165.24	9.11	Lick
11,213.786..........	−151.93	9.58	Lick
11,226.830..........	−141.17	3.61	Keck
11,227.758..........	−135.70	3.24	Keck
11,228.852..........	−122.18	2.81	Keck
11,229.774..........	−114.00	3.36	Keck
11,454.021..........	−134.30	4.95	Lick
11,455.030..........	−110.09	7.93	Lick
11,468.050..........	−149.67	8.14	Lick
11,468.963..........	−136.97	7.15	Lick
11,482.983..........	−118.32	6.34	Lick
11,496.929..........	−121.39	8.12	Lick
11,532.852..........	−25.50	4.87	Lick
11,533.862..........	−17.89	4.08	Lick
11,534.898..........	−6.99	5.47	Lick
11,535.881..........	−31.07	5.40	Lick
11,536.829..........	−59.03	5.97	Lick
11,539.931..........	−111.38	6.53	Lick
11,540.870..........	−99.30	5.08	Lick
11,543.791..........	−53.17	8.30	Lick
11,546.832..........	−9.76	9.56	Lick
11,550.879..........	−34.70	3.49	Keck
11,551.909..........	−81.10	3.06	Keck
11,552.857..........	−102.74	2.78	Keck
11,571.753..........	−81.49	8.08	Lick
11,572.654..........	−61.26	7.57	Lick
11,573.713..........	−58.46	11.48	Lick
11,580.847..........	−86.84	3.01	Keck
11,581.690..........	−124.22	6.49	Lick
11,581.757..........	−102.36	3.31	Keck
11,582.792..........	−100.49	3.12	Keck
11,583.913..........	−87.25	3.63	Keck
11,584.750..........	−83.50	2.42	Keck
11,585.909..........	−60.50	3.45	Keck
11,593.798..........	−37.37	7.56	Lick
11,607.733..........	−13.22	6.50	Lick
11,629.655..........	−46.88	6.47	Lick
11,793.121..........	72.21	3.69	Keck
11,815.021..........	3.53	7.03	Lick
11,817.021..........	44.01	5.77	Lick
11,823.025..........	41.26	4.95	Lick
11,824.024..........	−5.55	6.99	Lick
11,825.032..........	−28.13	6.52	Lick
11,826.024..........	−25.87	5.63	Lick
11,827.013..........	−10.16	6.86	Lick

TABLE 6—Continued

JD − 2,440,000	RV (m s^{-1})	Uncertainties (m s^{-1})	Observatory
11,831.021..........	59.01	4.77	Lick
11,832.008..........	71.49	4.87	Lick
11,834.966..........	96.82	4.59	Lick
11,837.014..........	56.24	7.57	Lick
11,838.035..........	15.25	6.41	Lick
11,840.015..........	−23.59	7.30	Lick
11,841.978..........	−0.01	5.70	Lick
11,859.960..........	71.10	5.79	Lick
11,860.923..........	81.42	6.05	Lick
11,866.032..........	63.25	7.02	Lick
11,868.987..........	−0.01	5.65	Lick
11,874.913..........	76.04	5.31	Lick
11,875.950..........	97.18	14.57	Lick
11,879.913..........	74.97	7.36	Lick
11,880.956..........	31.00	5.30	Lick
11,882.943..........	0.00	3.49	Keck
11,884.089..........	13.61	3.19	Keck
11,894.903..........	45.10	9.68	Lick
11,898.074..........	26.03	3.33	Keck
11,899.048..........	33.61	3.19	Keck
11,900.068..........	54.51	3.23	Keck
11,905.869..........	118.29	5.15	Lick
11,906.843..........	123.55	5.07	Lick
11,907.846..........	108.80	6.17	Lick
11,913.801..........	43.43	3.75	Lick
11,914.854..........	54.69	4.00	Lick
11,915.814..........	78.71	3.94	Lick
11,927.814..........	41.65	4.09	Lick
11,945.737..........	102.25	3.92	Lick
11,946.705..........	113.55	4.40	Lick
11,973.750..........	122.55	8.46	Keck
11,974.767..........	137.78	8.34	Keck
12,003.750..........	163.11	8.22	Keck
12,007.762..........	194.95	3.38	Keck
12,134.136..........	266.66	3.72	Keck
12,162.014..........	254.42	5.57	Lick
12,188.147..........	214.79	3.77	Keck
12,218.983..........	241.55	3.51	Keck
12,220.083..........	245.57	4.48	Keck
12,235.890..........	271.74	3.42	Keck
12,236.911..........	262.27	3.69	Keck
12,238.897..........	186.99	3.70	Keck
12,242.935..........	189.41	3.45	Keck
12,262.926..........	246.72	5.73	Lick
12,278.874..........	282.96	6.84	Lick
12,279.762..........	262.40	5.34	Lick
12,281.883..........	178.61	9.30	Lick
12,285.867..........	187.64	6.24	Lick
12,287.803..........	221.97	7.52	Lick
12,292.835..........	228.85	7.06	Lick
12,293.808..........	239.00	5.74	Lick
12,294.801..........	206.41	7.52	Lick
12,306.676..........	240.92	5.03	Lick
12,307.814..........	257.21	3.39	Keck
12,314.719..........	157.63	5.34	Lick
12,315.712..........	161.02	4.34	Lick
12,333.685..........	207.87	6.73	Lick
12,334.653..........	222.72	6.22	Lick
12,334.776..........	229.78	4.20	Keck
12,516.137..........	8.88	3.45	Keck
12,536.103..........	63.77	3.50	Keck

NOTE.—Table 6 is also available in machine-readable form in the electronic edition of the *Astrophysical Journal*.

TABLE 7
ORBITAL PARAMETERS FOR HD 38529

Parameter	HD 38529b	HD 38529c
P (d)	14.309 (0.05)	2174.3 (30.0)
T_p (JD)................	2,450,005.8 (1.5)	2,450,073.8 (35.0)
e.........................	0.29 (0.02)	0.36 (0.05)
ω (deg).................	87.7 (4..0)	14.7 (10.0)
K_1 (m s^{-1})............	54.2 (1.2)	170.5 (9.0)
$a_1 \sin i$ (AU)........	6.8E−05	3.18E−02
$f_1(m)$ ($M_\odot$)...........	2.07E−10	9.10E−07
a_{rel} (AU)..............	0.129	3.68
$M \sin i$ (M_{Jup})	0.78	12.70
N_{obs}....................	...	125
rms (m s^{-1})..........	...	10.99
Reduced $(\chi^2)^{1/2}$...	...	2.08

be associated with low-amplitude photometric variability. The rms variability of the entire photometric data set is 0.0024 mag. Analysis by one of us (G. W. H.) shows that this level of photometric variability is empirically only correlated with about 8 m s^{-1} of radial velocity variability because of surface activity in a main-sequence star.

The double-Keplerian fit for HD 38529 shows an rms scatter of 10.99 m s^{-1} with a reduced $(\chi^2)^{1/2}$ of 2.08. This scatter is clearly seen in the higher precision Keck data as
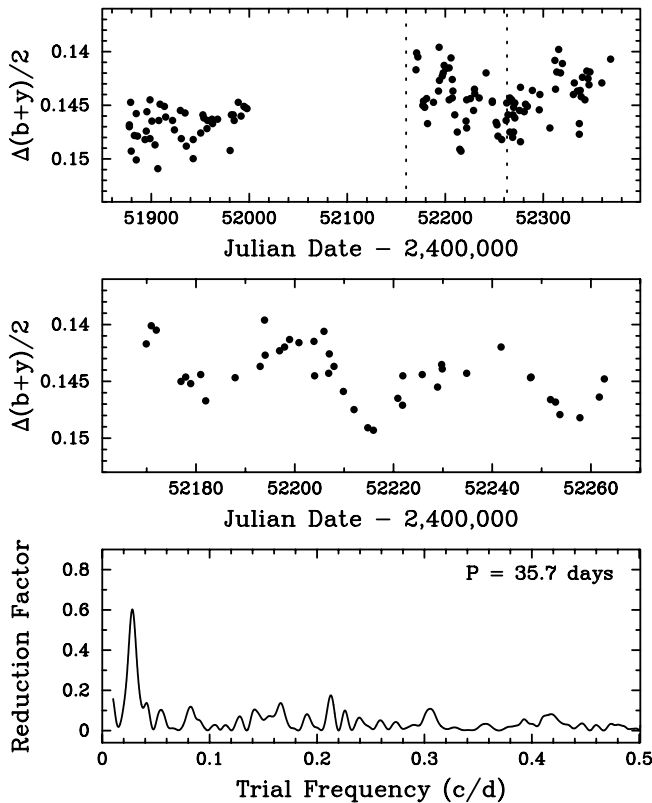

FIG. 8.—Photometry of HD 38529 acquired with the T11 0.8 m APT at Fairborn Observatory. The top panel shows the entire data set. The subset between the dashed vertical lines, replotted in the middle panel, shows the most coherent rotational modulation in the star's brightness. Period analysis of this subset is shown in the bottom panel and reveals a clear rotation signal of 35.7 ± 1.1 days, very close to the 34.5 day rotation period predicted from the star's H and K emission but very different from the 14.309 and 2174.3 day periods of the two planetary companions.
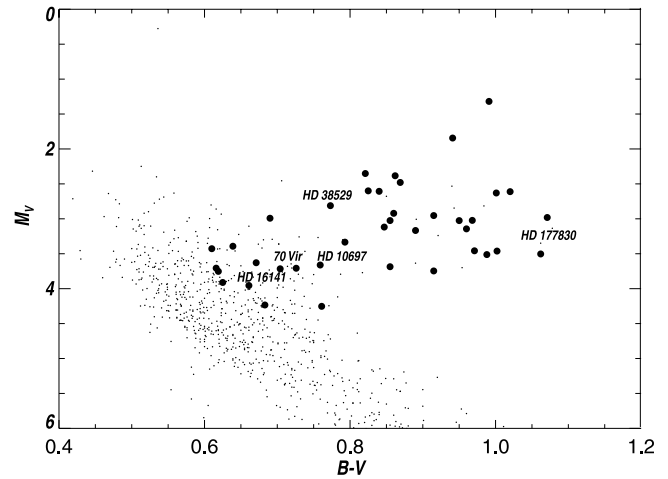

FIG. 9.—Color-magnitude diagram for our planet search targets. The bold dots highlight subgiants in our project with more than three velocity observations. The labeled dots represent stars where extrasolar planets have been detected.

well as in the Lick data and is greater than expected for a slowly rotating, chromospherically inactive star. The rms scatter (rather than the larger amplitude Keplerian variations) could be related to the photometric variability; however, a periodogram of the residuals to the double-Keplerian fit does not show any power near 20–40 days.

It is also possible that the moderately high velocity rms is related to the subgiant status of the star. To investigate this, we examined the rms velocity scatter for other subgiants on our planet search surveys. Figure 9 shows a color-magnitude diagram for our planet search targets. The bold dots indicate stars with more than three radial velocity measurements that also appear to be on the subgiant branch. The labeled points in Figure 9 are subgiants with detected extrasolar planets. Figure 10 shows the rms velocity scatter of the subgiants in Figure 9. In the case of the stars with planets,
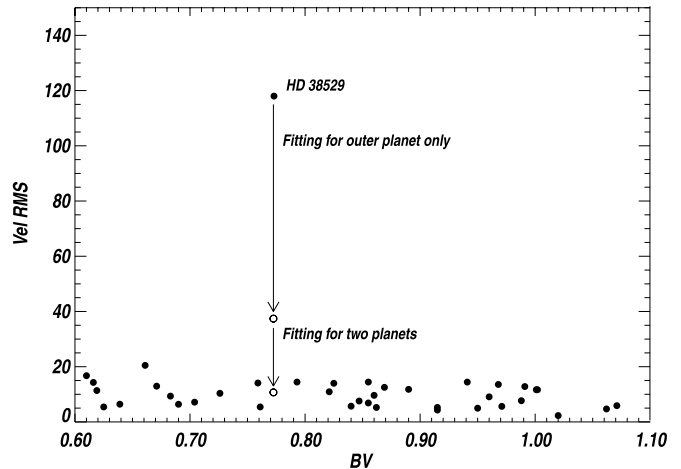

FIG. 10.—Velocity rms for subgiants indicated with bold dots in Fig. 8. For HD 16141, HD 10697, HD 177830, and 70 Vir, the velocity rms refers to the residual velocities, after fitting for the known planets. The velocity rms for HD 38529 is shown as a series of points. The high rms point is the velocity rms without fitting for any planets. After fitting for the dominant, long-period orbit, the rms of the residual velocities drops to about 40 m s^{-1}. After fitting for both of the planets described in this paper, the residual velocity rms drops to about 10 m s^{-1}, consistent with the rms of other subgiants on our projects.

the rms scatter is the residual rms to a Keplerian model. There are three points for HD 38529 indicated in Figure 10: the highest point is the rms of all of the velocities (no Keplerian fitting), the intermediate point shows the rms after fitting a single Keplerian to the dominant long-period orbit, and the lowest point shows the rms to the double-Keplerian fit. So, after fitting two Keplerians, the rms of HD 38529 appears to show scatter typical in magnitude to other subgiants. To further investigate the origin of the scatter in subgiants, we plotted the rms velocities against both absolute magnitude and color, but no correlation was apparent. A larger data set may be helpful in understanding the effects of evolution on radial velocity jitter. The radial velocity study of class III K giants (Frink et al. 2001) shows that for $B-V$ blueward of 1.1, the typical rms velocity scatter is less than 40 m s^{-1}. So, velocity jitter is less than a few meters per second in chromospherically inactive stars, it is less than 20 m s^{-1} in class IV subgiants, and it is less than 40 m s^{-1} in class III giant stars that are bluer than $B-V = 1.1$. Redward of $B-V = 1.1$, Figure 5 in Frink et al. (2001) shows a dramatic rise to more than 100 m s^{-1} in rms jitter for red giant stars.

3. DISCUSSION

The companion to HD 40979 has an orbital period of 263 days, eccentricity of 0.25, and $M \sin i = 3.28 M_{\rm Jup}$. The star exhibits moderate chromospheric activity ($\log R'_{\rm HK} = -4.63$). Photometric observations reveal low-amplitude brightness variations in HD 40979 due to rotational modulation by photospheric starspots, and they yield a rotation period of 7.0 ± 0.5 days, very different from the planetary orbital period. HD 40979 is a metal-rich star with $[{\rm Fe/H}] = 0.194$, typical of stars that host Doppler-detected gas giant planets (Gonzalez 1998; Fischer & Valenti 2003).

HD 12661 hosts two extrasolar planets. The inner planet has an orbital period of 263 days, eccentricity of 0.35, and

$M \sin i = 2.3 M_{\rm Jup}$. The outer planet has an orbital period of 1444 days, eccentricity of 0.20, and $M \sin i = 1.57 M_{\rm Jup}$. The star is chromospherically inactive, photometrically stable, and metal-rich, with $[{\rm Fe/H}] = 0.29$.

We have also detected a second planet orbiting HD 38529. The inner companion has an orbital period of 14.3 days, eccentricity of 0.29, and $M \sin i = 0.78 M_{\rm Jup}$. The outer companion has an orbital period of 2174 days, eccentricity of 0.36, and $M \sin i = 12.70 M_{\rm Jup}$. The star is a subgiant with metallicity $[{\rm Fe/H}] = 0.36$. HD 38529 shows photometric variability at the millimagnitude level that yields a rotation period of 35.7 days. However, this low-level variability has a different periodicity from the strong velocity amplitudes that we interpret as Keplerian signals.

We searched for evidence of the long-period orbits for HD 12661 and HD 38529 in the *Hipparcos* astrometric data. However, after refitting the *Hipparcos* intermediate data with the orbital parameters from this paper, we were unable to obtain an improved statistical fit to the *Hipparcos* observations for HD 40979, HD 12661, or HD 38529. The lack of a *Hipparcos* detection offers only a weak upper limit on the companion mass but nevertheless constrains all three of the companions presented here to the substellar mass regime.

3.1. *Multiple-Planet Systems*

The detection of additional planets orbiting HD 12661 and HD 38529 raises to 10 the number of multiple-planet systems that have been discovered. Updated orbital properties of these multiple-planet systems are listed in Table 8.

Three years have passed since the triple-planet system was discovered orbiting Υ And. In order to improve the dynamical modeling of that system, we have continued to observe Υ And frequently at Lick Observatory. In Table 9, 159 new radial velocities have been added to the original 89 velocities published in Butler et al. (1999). These new

TABLE 8
PROPERTIES OF THE 10 KNOWN MULTIPLE-PLANET SYSTEMS

Star	$M_{\rm star}$ ($M_\odot$)	P (days)	K (m s^{-1})	Eccentricity	$M \sin i$ ($M_{\rm Jup}$)	a (AU)	Last Velocity Update	Comment
Υ And b	1.30	4.617	70.15	0.01	0.64	0.058	2002 Nov 22	
Υ And c	1.30	241.16	53.93	0.27	1.79	0.805		Apsidal lock
Υ And d	1.30	1276.15	60.62	0.25	3.53	2.543		Apsidal lock
55 Cnc b	1.03	14.653	71.7	0.03	0.83	0.115	2002 Oct 28	3 : 1 resonance
55 Cnc c	1.03	44.27	13.2	0.41	0.20	0.241		3 : 1 resonance
55 Cnc d	1.03	4780	48.0	0.28	3.69	5.461		
GJ 876 b	0.32	61.020	210.0	0.10	1.89	0.207	2002 Oct 28	2 : 1 mean motion
GJ 876 c	0.32	30.120	81.0	0.27	0.56	0.130		Resonance
47 UMa b	1.03	1079.2	55.6	0.05	2.86	2.077	2002 Nov 22	8 : 3 commensurability?
47 UMa c	1.03	2845.0	15.7	0.00	1.09	3.968		8 : 3 commensurability?
HD 168443 b...	1.01	58.1	470.0	0.53	7.64	0.295	2002 Oct 27	
HD 168443 c ...	1.01	1770.0	289.0	0.20	16.96	2.873		
HD 37124 b.....	0.91	153.3	35.0	0.10	0.86	0.543	2002 Oct 27	
HD 37124 c	0.91	1942.0	19.0	0.40	1.00	2.952		
HD 12661 b.....	1.07	263.6	74.4	0.35	2.30	0.823	This paper	Secular resonance
HD 12661 c	1.07	1444.5	27.6	0.20	1.57	2.557		Secular resonance
HD 38529 b.....	1.39	14.309	54.2	0.29	0.78	0.129	This paper	
HD 38529 c	1.39	2174.3	170.5	0.36	12.7	3.68		
HD 82943 b.....	1.05	444.6	46.0	0.41	1.63	1.159	2002 Jul 31[a]	2 : 1 resonance
HD 82943 c	1.05	221.6	34.0	0.54	0.88	0.728		2 : 1 resonance
HD 74156 b.....	1.05	51.6	112.0	0.65	1.61	0.278	2002 Aug 5[a]	
HD 74156 c	1.05	>2650	125.0	0.35	>8.21	>3.82		

[a] The velocities and orbital parameters for HD 82943 and HD 74156 have not yet been published; values taken from http://obswww.unige.ch.

TABLE 9
Radial Velocities for Υ Andromedae
(Lick Observatory)

JD − 2,440,000	RV (m s⁻¹)	Uncertainties (m s⁻¹)
7046.922.............	133.55	14.59
7093.759.............	−10.83	16.70
7094.762.............	5.06	14.32
7149.778.............	−114.76	13.11
7193.629.............	−6.33	10.80
8845.965.............	68.44	16.70
8855.934.............	117.55	11.29
8891.935.............	−3.79	9.89
8907.838.............	9.61	10.47
8933.828.............	22.19	9.35
8935.848.............	5.46	11.06
9255.855.............	6.89	14.34
9298.803.............	101.21	10.12
9350.706.............	69.47	13.54
9588.992.............	−12.36	9.78
9602.962.............	−44.14	15.74
9622.928.............	11.45	16.13
9680.753.............	−122.03	6.76
9942.008.............	15.07	9.25
9969.979.............	−13.64	6.44
9984.852.............	−53.79	6.74
10,032.741.............	37.52	8.06
10,056.842.............	57.42	6.34
10,068.586.............	−58.49	7.15
10,068.773.............	−56.98	7.67
10,069.599.............	23.04	11.35
10,072.603.............	−87.12	9.82
10,072.724.............	−90.65	8.67
10,073.652.............	−60.45	8.62
10,080.783.............	−21.50	11.37
10,086.739.............	−93.88	9.45
10,087.689.............	−25.68	9.64
10,088.741.............	46.47	8.87
10,089.710.............	5.00	9.00
10,090.646.............	−76.97	5.52
10,091.663.............	−81.19	9.96
10,299.008.............	3.34	9.95
10,305.992.............	140.20	7.98
10,310.001.............	108.46	9.52
10,310.996.............	114.75	8.48
10,311.984.............	46.79	8.26
10,325.891.............	−51.30	8.92
10,326.914.............	−28.72	8.60
10,327.918.............	31.97	7.86
10,372.958.............	−45.64	11.04
10,373.839.............	−9.52	7.54
10,374.884.............	71.88	11.42
10,376.910.............	−24.68	11.39
10,377.811.............	−67.76	10.91
10,421.568.............	149.68	7.31
10,421.756.............	138.84	6.80
10,437.686.............	34.78	6.82
10,437.870.............	49.52	10.38
10,441.771.............	42.02	7.10
10,640.983.............	−51.10	8.92
10,655.995.............	72.59	8.71
10,656.945.............	107.65	8.41
10,681.982.............	1.64	9.27
10,767.728.............	102.63	11.21
10,793.716.............	−32.19	9.12
10,977.996.............	−70.20	11.00

TABLE 9—Continued

JD − 2,440,000	RV (m s⁻¹)	Uncertainties (m s⁻¹)
10,979.992...........	73.39	8.79
11,014.980...........	−108.37	7.88
11,025.971...........	8.91	7.82
11,026.954...........	−22.16	7.60
11,028.007...........	−122.95	7.96
11,045.019...........	−7.04	8.28
11,046.007...........	−95.49	9.23
11,046.985...........	−149.95	8.46
11,047.957...........	−98.88	8.18
11,048.932...........	−16.27	5.72
11,049.917...........	−32.05	5.73
11,074.914...........	−176.86	7.97
11,076.903...........	−32.78	8.27
11,100.904...........	−95.28	9.65
11,101.878...........	−174.09	9.66
11,130.855...........	−110.87	10.56
11,131.799...........	−7.03	9.52
11,132.721...........	4.40	10.96
11,133.840...........	−81.93	11.73
11,154.726...........	1.48	10.31
11,174.670...........	−3.13	10.72
11,175.607...........	−80.35	10.12
11,206.645...........	33.49	8.10
11,212.674...........	−106.28	11.47
11,213.666...........	−104.67	10.25
11,239.635...........	−46.74	7.70
11,240.646...........	−119.88	8.01
11,242.635...........	−1.45	7.87
11,351.984...........	−116.07	8.66
11,353.963...........	−1.23	10.33
11,354.952...........	−59.22	9.54
11,362.979...........	15.45	5.67
11,363.990...........	−19.63	7.01
11,364.975...........	−88.04	8.37
11,375.972...........	0.86	8.41
11,376.995...........	66.29	7.94
11,377.951...........	35.21	4.68
11,378.971...........	−46.68	4.55
11,379.975...........	−45.52	4.93
11,380.963...........	51.47	8.10
11,386.984...........	72.61	5.99
11,387.984...........	−8.13	4.97
11,388.984...........	−39.42	5.69
11,389.988...........	48.61	5.84
11,392.000...........	42.58	8.54
11,392.984...........	−33.82	6.20
11,401.936...........	19.90	9.26
11,402.884...........	3.10	6.00
11,403.920...........	91.60	5.71
11,405.976...........	66.68	8.78
11,406.993...........	−4.66	8.16
11,408.023...........	40.63	8.43
11,409.985...........	111.33	7.35
11,416.785...........	6.88	5.82
11,416.978...........	19.73	5.53
11,417.800...........	93.70	6.67
11,418.935...........	129.50	5.23
11,419.900...........	57.41	5.68
11,425.950...........	9.33	6.13
11,426.953...........	85.42	8.88
11,427.955...........	151.24	5.64
11,428.934...........	90.52	7.40
11,429.973...........	3.46	5.93

TABLE 9—*Continued*

JD − 2,440,000	RV (m s^{-1})	Uncertainties (m s^{-1})
11,435.954..........	82.29	5.76
11,436.802..........	152.96	7.36
11,437.975..........	106.39	7.66
11,438.897..........	39.25	6.30
11,439.873..........	28.56	5.73
11,440.856..........	113.75	6.82
11,444.981..........	64.41	6.59
11,445.922..........	132.73	6.58
11,446.943..........	120.47	6.46
11,447.934..........	31.09	6.94
11,453.862..........	45.87	6.00
11,454.808..........	113.07	6.64
11,467.859..........	27.60	6.10
11,468.831..........	130.35	5.64
11,477.863..........	103.83	10.23
11,478.833..........	120.44	10.08
11,481.817..........	50.22	13.96
11,482.802..........	136.30	6.28
11,496.710..........	128.69	8.09
11,500.807..........	88.41	9.14
11,501.706..........	130.36	9.11
11,533.726..........	83.67	7.57
11,539.664..........	44.16	7.89
11,540.687..........	−40.32	9.40
11,542.642..........	60.70	10.06
11,543.636..........	87.22	10.12
11,572.597..........	−47.93	10.55
11,573.661..........	−72.54	10.85
11,581.613..........	−28.24	10.09
11,734.002..........	25.43	5.26
11,738.996..........	−9.69	8.03
11,740.003..........	−4.24	8.15
11,742.988..........	33.75	7.44
11,743.985..........	−22.70	7.74
11,744.986..........	16.12	8.56
11,745.986..........	101.72	7.65
11,746.975..........	93.70	9.17
11,751.001..........	98.73	5.14
11,752.997..........	−31.13	4.42
11,774.947..........	48.64	4.34
11,775.978..........	−47.74	4.44
11,778.956..........	72.23	4.39
11,780.958..........	−63.49	4.42
11,782.979..........	67.24	4.90
11,798.943..........	−75.43	6.96
11,802.946..........	−4.92	5.50
11,803.955..........	−74.64	5.45
11,804.934..........	−34.43	5.19
11,805.875..........	49.19	5.88
11,806.915..........	52.86	6.98
11,813.819..........	−77.92	4.74
11,814.880..........	13.71	5.02
11,815.916..........	49.94	7.36
11,816.800..........	−12.75	5.18
11,822.842..........	−79.62	6.97
11,823.820..........	−24.87	5.76
11,824.863..........	48.69	6.00
11,825.808..........	1.39	6.04
11,826.818..........	−86.02	7.58
11,830.823..........	−30.34	7.81
11,831.783..........	−86.59	7.74
11,837.788..........	−5.21	8.37
11,865.787..........	92.90	6.09
11,866.719..........	118.74	7.14

TABLE 9—*Continued*

JD − 2,440,000	RV (m s^{-1})	Uncertainties (m s^{-1})
11,877.763..........	−13.12	7.44
11,881.626..........	55.72	5.45
11,882.628..........	4.82	6.74
11,886.673..........	44.69	8.54
11,887.665..........	5.92	7.09
11,891.763..........	0.54	5.94
11,895.652..........	23.54	10.48
11,896.713..........	10.03	11.35
12,111.937..........	37.97	6.32
12,120.937..........	76.07	6.26
12,121.895..........	−3.52	5.78
12,124.962..........	101.39	8.74
12,129.892..........	90.76	5.45
12,145.907..........	−38.85	7.42
12,146.911..........	14.19	5.96
12,147.824..........	81.14	6.46
12,148.945..........	62.23	7.48
12,156.879..........	72.90	7.34
12,157.908..........	74.28	5.22
12,158.937..........	−17.08	5.78
12,159.898..........	−41.50	5.12
12,160.906..........	32.03	8.59
12,161.901..........	104.24	8.66
12,162.808..........	56.68	9.22
12,167.801..........	24.63	6.37
12,181.823..........	13.11	6.60
12,187.792..........	−44.83	5.67
12,219.819..........	−91.74	7.75
12,221.683..........	46.22	7.92
12,251.638..........	−128.65	7.65
12,256.645..........	−134.87	6.84
12,262.656..........	−52.03	7.52
12,278.616..........	−110.20	7.44
12,281.636..........	−59.71	7.09
12,491.915..........	−137.32	5.88
12,492.963..........	−105.65	5.61
12,493.942..........	−10.34	5.33
12,508.943..........	−46.00	5.41
12,509.857..........	−124.46	5.85
12,511.972..........	−71.68	5.27
12,512.950..........	−18.24	5.44
12,513.943..........	−88.60	5.39
12,515.911..........	−106.71	5.75
12,520.921..........	−103.64	6.36
12,522.889..........	−59.41	5.63
12,524.903..........	−163.48	5.91
12,534.878..........	−94.64	5.79
12,540.927..........	−46.89	6.38
12,552.873..........	−151.50	6.82
12,553.827..........	−57.16	6.43
12,554.814..........	−36.70	6.99
12,563.899..........	−12.15	6.04
12,564.949..........	−83.83	5.71
12,567.018..........	−81.75	6.63
12,570.768..........	−134.08	6.80
12,574.781..........	−102.86	7.69
12,575.733..........	−89.80	6.98
12,593.754..........	−74.31	7.09
12,594.779..........	−5.51	6.56
12,597.740..........	−49.81	7.28

NOTE.—Table 9 is also available in machine-readable form in the electronic edition of the *Astrophysical Journal*.

velocities better constrain the orbital eccentricity of the outer planet in that system. Fitting 16 free orbital parameters simultaneously, our updated orbital parameters for the inner planet are $P_b = 4.6171 \pm 0.0001$ days, $Tp_b = 2451807.7 \pm 1.2$ days, $e_b = 0.019 \pm 0.02$, and $K_b = 70.9 \pm 2.1$ m s^{-1}. The best-fit parameters for the middle planet are $P_c = 241.18 \pm 0.5$ days, $Tp_c = 2450160.7 \pm 6.6$ days, $\omega_c = 249.1 \pm 9.3$, $e_c = 0.26 \pm 0.03$, and $K_c = 53.0 \pm 2.0$ m s^{-1}. The best-fit parameters for the outer planet are $P_d = 1282.60 \pm 11.5$ days, $Tp_d = 2450075.3 \pm 45.6$ days, $\omega_d = 264.2 \pm 17.2$, $e_d = 0.25 \pm 0.03$, and $K_d = 60.9 \pm 2.1$ m s^{-1}. The rms to the triple-Keplerian fit is 14.5 m s^{-1}, consistent with the measurement uncertainty from the combination of the measurement error (9 m s^{-1} because of rotational line broadening) and the expected stellar jitter (10 m s^{-1}). We do not find any evidence for a residual velocity trend to the triple-Keplerian fit in our 15 yr set of Lick Observatory velocities. Figure 11a shows the phased velocity curve for Υ And b with velocities of the outer two components removed, and Figure 11b shows the stellar velocities arising from the outer two planets after subtracting velocities from the inner planet.

Velocities from two additional seasons of observations for 47 UMa now yield an improved eccentricity and orbital period for the outermost planet. The orbital period ratio of the two planets orbiting 47 UMa is now close to the 8 : 3 commensurability. Fitting for 11 free orbital parameters simultaneously, the best-fit solution for the inner planet is $P_b = 1079.14 \pm 6.2$ days, $Tp_b = 2452374.1 \pm 26.6$ days, $\omega_b = 124.3 \pm 12.7$, $e_b = 0.05 \pm 0.04$, and $K_b = 54.7 \pm 4.2$ m s^{-1}. The best-fit Keplerian solution for the outer planet is $P_c = 2845.0 \pm 60$ days, $Tp_c = 2448750.9 \pm 86$ days, $\omega_c = 170.8 \pm 15.3$, $e_c = 0.00 \pm 0.03$, and $K_c = 15.7 \pm 1.8$ m s^{-1}. The Keplerian models for the individual components are shown in Figures 12a and 12b. The rms to the double-Keplerian fit is 5.5 m s^{-1}. The nearly circular orbit of the outermost planet has a derived orbital radius of about 4 AU and an $M_c \sin i$ of $1.1 M_{\rm Jup}$, making this planet a *strikingly close analog of Jupiter in our own solar system*.

Marcy et al. (2003) have introduced the classification "hierarchical" for widely separated double-planet systems.

They arbitrarily define hierarchical planetary systems as those in which the ratio of orbital periods (P_2/P_1) is greater than 5 : 1. Such systems are less likely to be actively engaged in mean motion or secular resonances. Any resonances that persist in hierarchical systems act on timescales that are long compared to both the orbital periods and human observations.

There are eight double-planet systems and two triple-planet systems listed in Table 8. Among these 10 multiple-planet systems, 10 component pairs are hierarchical and four component pairs have $P_2/P_1 < 5$. Apsidal locking is apparent between the hierarchical planet components Υ And b and c (Chiang & Murray 2002; Chiang, Tabachnik, & Tremaine 2001), and Lee & Peale (2003) calculate that the hierarchical system HD 12661 is in a secular resonance. None of the 20 hierarchical pairs are in a mean motion resonance. In contrast, three of the four systems with $P_2/P_1 < 5$ exhibit mean motion resonance: GJ 876 (2 : 1), HD 82943 (2 : 1), and 55 Cnc (3 : 1), and the updated orbital parameters for 47 UMa suggest that the two planets in this system are near the 8 : 3 commensurability. So, empirically, resonances are an important characteristic in systems with $P_2/P_1 < 5$ but of less importance in the architecture of more widely spaced hierarchical systems.

HD 38529 highlights an interesting feature of hierarchical planet systems. Because the outer planet is clearly the more massive, it is unlikely that the inner planet scattered the outer planet to its current orbit. The semi-major axes of the two planets were probably not set by planet-planet interactions. Using a Bulirsch-Stoer integrator, we ran 10 Myr integrations of the HD 12661 and HD 38529 systems. The planets remained in stable orbits throughout the simulations, with only a mild, periodic eccentricity exchange between the component planets. Thus, the significant orbital eccentricities (0.29 and 0.36 for the inner and outer planets, respectively) of the two planets around HD 38529 may have arisen by some other mechanism than mutual interactions. A possible origin for the observed eccentricities is perturbation by either the protoplanetary disk or an orbiting stellar companion.
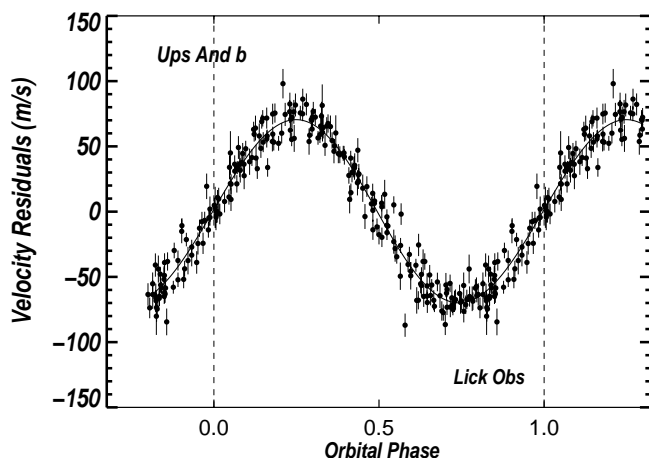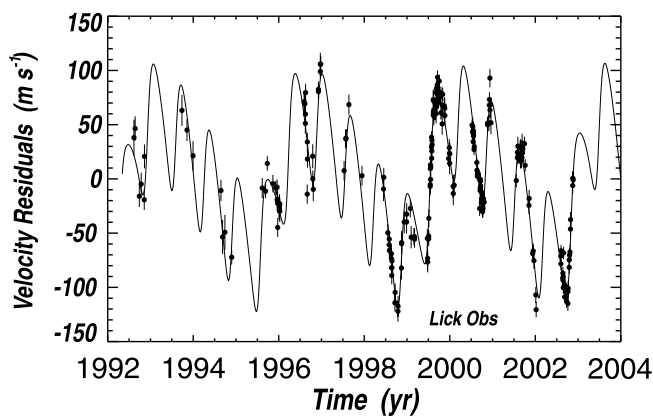

Fig. 11a

Fig. 11b

Fig. 11.—Radial velocities for Υ And from Lick Observatory. The solid lines show the Keplerian models. (*a*) Phased velocities for the inner planet after subtracting the Keplerian fit to the outer two planets. $P_b = 4.6171$ days, $e_b = 0.019$, $K_b = 70.9$ m s^{-1}, and $M_b \sin i = 0.71 M_{\rm Jup}$. (*b*) Stellar velocities from the outer two planets after subtracting theoretical velocities for the inner planet. $P_c = 241.18$, $e_c = 0.26$, $K_c = 53.0$ m s^{-1}, $M_c \sin i = 1.98 M_{\rm Jup}$, $P_d = 1282.6$, $e_d = 0.25$, $K_d = 60.9$ m s^{-1}, and $M_d \sin i = 3.9 M_{\rm Jup}$.
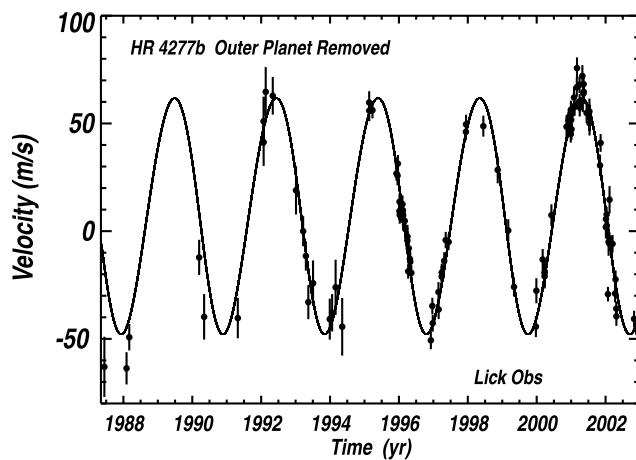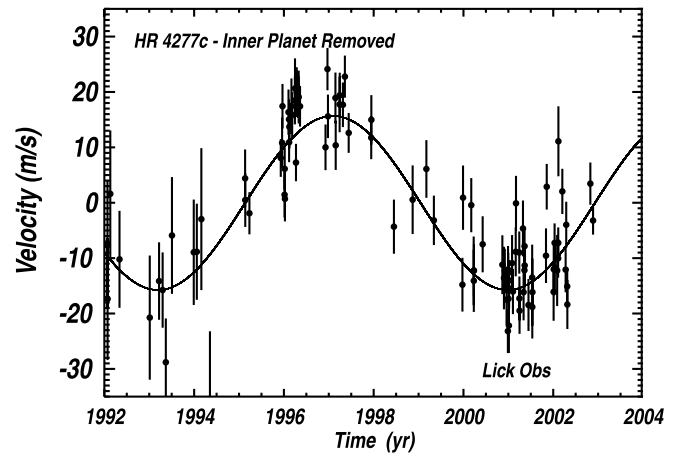
FIG. 12a

FIG. 12b

FIG. 12.—Radial velocities of 47 UMa from Lick Observatory. (*a*) Velocities from the inner planet are shown by subtracting the Keplerian fit to the outer planet. $P_b = 1079$ days, $e_b = 0.05$, $K_b = 54.7$ m s^{-1}, and $M_b \sin i = 2.9 M_{\rm Jup}$. (*b*) Velocities from the outer planet are revealed by subtracting theoretical velocities for the inner planet. $P_c = 2845$ days, $e_c = 0.0$, $K_c = 15.7$ m s^{-1}, and $M_c \sin i = 1.1 M_{\rm Jup}$.

Many single planets also reside in highly eccentric orbits without additional massive planets or stars currently known to be orbiting the host star. The stars 14 Her and 70 Vir both have massive planets in eccentric orbits, but the velocities over the past decade show no evidence of additional companions. This suggests that high eccentricities in planetary or stellar systems can occur without benefit of an additional, current companion.

Are eccentricities pumped in single planets by a different mechanism than in multiple-planet systems? To investigate this, one may compare the eccentricity distributions among single- and multiple-planet systems. Figure 13 shows orbital eccentricity versus semimajor axis for all 97 securely known planet systems. The eccentricities in Figure 13 show several remarkable features. The eccentricities are distributed from 0 to 0.71, with only one case (HD 80606, likely caused by its stellar companion) above that upper limit. An explanation has not been provided for this upper limit to the orbital
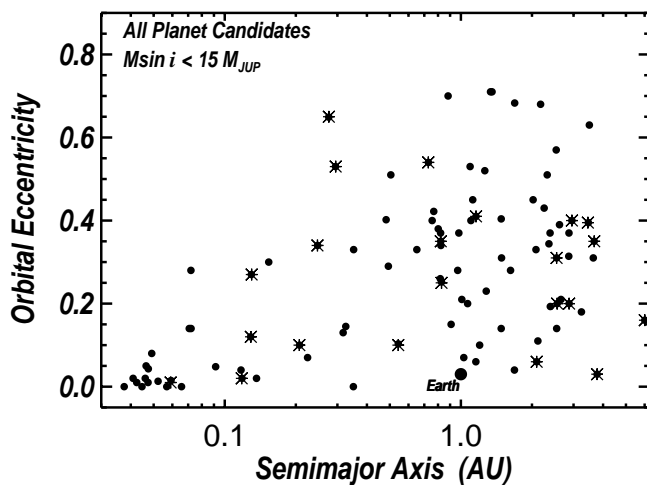

FIG. 13.—Eccentricity vs. semimajor axis for all known extrasolar planets. Planets in multiple-planet systems are displayed with asterisks. Eccentricities scatter between 0.0 and 0.7, with an apparent upper limit at $e = 0.7$ and an increasing upper envelope between $a = 0.1$ and 0.5. Planets in multiple-planet systems have eccentricities similar to those of single planets. (HD 80606b, with $e = 0.93$, sits off the plotted range.)

eccentricities of planetary orbits. Moreover, for semimajor axes between 0.1 and 1.0 AU, there appears to be an upper envelope of eccentricities that increases as the semimajor axis increases. In particular, there is a paucity of eccentricities between 0.3 and 0.7 for orbits having $a < 1.0$ AU. In contrast, for $a > 1.0$ AU, the most probable eccentricity is 0.35–0.45, as seen in Figure 13. Both the upper envelope to eccentricities at $e = 0.7$ and the trend in eccentricities for $a < 1.0$ AU await theoretical explanation.

Figure 13 also shows, with asterisks, those planets that reside in multiple-planet systems. There are 22 such planets, residing in 10 multiple systems, two of which are triples. *The distribution of orbital eccentricities among the planets in multiple-planet systems is indistinguishable from that of the single planets.* The similarity in the eccentricities of single planets and multiple planets suggests that the origin of the eccentricities may be the same. Such a similar mechanism would be remarkable because the planets in multiple-planet systems are definitely perturbed by each other, as seen dynamically in the GJ 876 system (Rivera & Lissauer 2001).

A selection effect may play a role in the high eccentricities observed among the *single* extrasolar planets discovered to date. Most known extrasolar planets reside within 3 AU because of the limited duration ($\sim$10 yr) of the Doppler surveys. Thus, the planets detected to date represent a subset that ended up within 3 AU. Giant planets within 3 AU may systematically represent the survivors of scattering events in which the other planet was ejected while extracting energy from the surviving planet and throwing it inward. We would systematically detect the more massive, surviving planet residing now in an orbit with period less than 10 yr.

Various mechanisms have been proposed to explain the orbital eccentricities, namely, planet-planet interactions, planet-disk interactions, and planet migration leading to resonance capture (Ford et al. 2003; Malhotra 2002; Marzari & Weidenschilling 2002; Lee & Peale 2002; Chiang & Murray 2002; Chiang, Fischer, & Thommes 2002; Goldreich & Sari 2003; Lin & Ida 1997). A comprehensive model for orbital eccentricities may include more than one process. Two or more planets will migrate in a viscous disk at different rates, allowing them to capture each other in mean motion resonances. Such resonances can then pump

the eccentricities of both planets up to values as high as 0.7 (Chiang 2003), as observed. The growth in eccentricities, especially as the disk dissipates, can render the two orbits unstable as close passages occur. Ford et al. (2003) show that such close passages often lead to ejection of the less massive planet, leaving one behind. This sequential set of processes provides a natural explanation for the resonances and eccentricities observed among multiple-planet systems and for the eccentricities observed in single planets. Single planets may simply represent the survivors of double-planet progenitors.

REFERENCES

Allende Prieto, C., & Lambert, D. L. 1999, A&A, 352, 555
Baliunas, S. L., Donahue, R. A., Soon, W., & Henry, G. W. 1998, in ASP Conf. Ser. 154, The 10th Cambridge Workshop on Cool Stars, Stellar Systems, and the Sun, ed. R. A. Donahue & J. A. Bookbinder (San Francisco: ASP), 153
Baliunas, S. L., et al. 1995, ApJ, 438, 269
Butler, R. P., Marcy, G. W., Fischer, D. A., Brown, T., Contos, A., Korzennik, S., Nisenson, P., & Noyes, R. W. 1999, ApJ, 526, 916
Butler, R. P., Marcy, G. W., Vogt, S. S., Fischer, D. A., Henry, G. W., Laughlin, G. P., & Wright, J. T. 2003, ApJ, 582, 455
Butler, R. P., Marcy, G. W., Williams, E., McCarthy, C., Dosanjh, P., & Vogt, S. S. 1996, PASP, 108, 500
Chiang, E. I. 2003, ApJ, 584, 465
Chiang, E. I., Fischer, D. A., & Thommes, E. 2002, ApJ, 564, L105
Chiang, E. I., & Murray, N. 2002, ApJ, 576, 473
Chiang, E. I., Tabachnik, S., & Tremaine, S. 2001, AJ, 122, 1607
Fischer, D. A., Marcy, G. W., Butler, R. P., Laughlin, G. P., & Vogt, S. S. 2002, ApJ, 564, 1028
Fischer, D. A., Marcy, G. W., Butler, R. P., Vogt, S. S., Frink, S., & Apps, K. 2001, ApJ, 551, 1107
Fischer, D. A., & Valenti, J. A. 2003, in ASP Conf. Ser., Scientific Frontiers in Research on Extrasolar Planets, ed. D. Deming & S. Seager (San Francisco: ASP), in press
Ford, E. B., Havlickova, M., Rasio, F. A., & Yu, K. 2003, Space Sci. Rev., in press
Frink, S., Quirrenbach, A., Fischer, D. A., Rösen, S., & Schilbach, E. 2001, PASP, 113, 173
Goldreich, P., & Sari, R. 2003, ApJ, 585, 1024
Gonzalez, G. 1998, A&A, 334, 221
Henry, G. W. 1999, PASP, 111, 845
Høg, E., et al. 2000, A&A, 355, L27
Jones, B. F., Fischer, D. A., & Soderblom, D. R. 1999, AJ, 117, 330
Laughlin, G. P., & Chambers, J. E. 2001, ApJ, 551, L109
Lee, M. H., & Peale, S. J. 2002, ApJ, 567, 596
———. 2003, ApJ, in press
Lin, D. N. C., & Ida, S. 1997, ApJ, 477, 781
Malhotra, R. 2002, ApJ, 575, L33
Marcy, G. W., Butler, R. P., Fischer, D. A., Laughlin, G. P., Vogt, S. S., Henry, G. W., & Pourbaix, D. 2002, ApJ, 581, 1375
Marcy, G. W., Butler, R. P., Fischer, D. A., & Vogt, S. S. 2003, Space Sci. Rev., in press
Marcy, G. W., Butler, R. P., Fischer, D. A., Vogt, S. S., Lissauer, J. J., & Rivera, E. J. 2001a, ApJ, 556, 296
Marcy, G. W., et al. 2001b, ApJ, 555, 418
Marzari, F., & Weidenschilling, S. 2002, Icarus, 156, 570
Mayor, M., & Queloz, D. 1995, Nature, 378, 355
Noyes, R. W., Hartmann, L., Baliunas, S. L., Duncan, D. K., & Vaughan, A. H. 1984, ApJ, 279, 763
Perryman, M. A. C. 1997, The *Hipparcos* and Tycho Catalogues (ESA-SP 1200; Noordwijk: ESA)
Queloz, D., et al. 2001, A&A, 379, 279
Rivera, E. J., & Lissauer, J. J. 2001, ApJ, 558, 392
Saar, S. H., Butler, R. P., & Marcy, G. M. 1998, ApJ, 498, L153
Vogt, S. S. 1987, PASP, 99, 1214
Vogt, S. S., et al. 1994, Proc. Soc. Photo-Opt. Instr. Eng., 2198, 362